Thin Solid Films 747 (2022) 139139

Contents lists available at ScienceDirect

Thin Solid Films

journal homepage: www.elsevier.com/locate/tsf

Optical, structural, and electrical properties of sputter-deposited SnO_x thin films

J.S. Jung [a], S.J. Park [b], J.H. Ye [a], J.G. Woo [c], B.S. Bae [c], E.-J. Yun [a,*]

[a] Department of Automotive ICT Engineering, Hoseo University, Dangjin, Chungnam, 31702, Republic of Korea
[b] Department of Materials Science and Engineering, Hoseo University, Asan, Chungnam, 31499, Republic of Korea
[c] Department of Display Engineering, Hoseo University, Asan, Chungnam, 31499, Republic of Korea

ARTICLE INFO

Keywords:
Thin films
Direct-current magnetron sputtering
Deposition parameters
p-type Tin oxide
Thermal annealing

ABSTRACT

This study investigated the effect of deposition parameters on the properties of tin oxide (SnO_x) thin films deposited by direct current magnetron sputtering using a Sn metal target. As confirmed by optical bandgap, X-ray photoelectron spectroscopy, high-resolution X-ray diffraction and Hall effect measurements, as-grown samples deposited at 7.5 and 10% oxygen partial pressure (OPP) and post-annealed samples deposited at 5% OPP had a p-type SnO phase, whereas samples fabricated with 7.5 and 10% OPP and annealed at 400°C had a n-type SnO_2 phase. Post-annealing at 400°C increases the bandgap and injects more oxygen into the SnO_x thin film, further oxidizing the sample. In addition, post-annealing greatly increased the carrier concentration of the SnO_x thin film, which increased carrier scattering and, in turn, greatly reduced the mobility of the sample. The SnO_x thin film deposited at 7.5% OPP and not heat treated showed the best p-type properties, with a Hall mobility of 5.11 cm^2/Vs, a hole carrier concentration of 1.13×10^{15} cm^{-3}, and a resistivity of 1082 Ωcm.

1. Introduction

Recently, tin-oxide (SnO_x) thin films have attracted great attention as hole or electron transport layers for solar cells [1–4] and organic light emitting diodes [5–7], as p- and n-type conductive layers for bipolar transistors, or as p- and n-type active layer of flexible oxide thin film transistors (TFTs) [8]. In addition, SnO_x thin films are promising candidates for producing complementary metal oxide semiconductor (CMOS) devices with high-performance n- and p-type oxide TFTs [9,10], thereby realizing a huge microelectronics revolution [11–18]. This is because the SnO_x film is a bipolar oxide semiconductor capable of both n- and p-type doping in the same SnO_x film. Furthermore, they exhibit low cost, thermal durability, chemical inertness, non-toxic features, natural abundance and mechanical stability [11–15,17–30].

Therefore, in order to implement a high-performance CMOS circuit, a high-performance p-type SnO_x is highly desirable. However, to date, the implementation of high-performance p-type SnO_x TFTs with high field-effect mobilities, sharp sub-threshold swings, and large on/off-drain current values is much more difficult [31]. This is mainly because the fabrication of SnO_x films with a single p-type SnO phase is still difficult.

Direct-current (DC) magnetron sputtering is the most effective process for fabricating large area devices, and it can easily produce multi-state oxides such as p-type SnO, n-type SnO_2 and metallic Sn. Understanding these multi-states is important because phase impurities always impede control of film performance. Nevertheless, the details of the microstructure, elemental and DC electrical transport characteristics of sputter-deposited SnO_x thin films are unclear, and the device characteristics of SnO_x-based TFTs are still not suitable for practical applications [32]. Therefore, in this study, we investigated the effect of oxygen partial pressure (OPP) on the properties of SnO_x thin films deposited by reactive DC magnetron sputtering on Sn metal targets.

2. Experimental details

SnO_x thin films were deposited on 400-μm-thick Si (100) (RNDKOREA Corp.) or soda-lime glass (Corning Inc.) substrates at a room temperature of 25 °C using a Sn (99.99%, 4 inch diameter) sputtering target under the following conditions: a DC power of 50 W, working pressure of 0.2 Pa, deposition times of 30 to 100 min, and oxygen partial pressures (OPPs) $[= \{\text{oxygen}/(\text{oxygen} + \text{argon})\} \times 100]$ of 0 to 10%. Pure argon (99.999%) and oxygen (99.999%) gas mixtures were used as the reaction gas and the total flow rate was 40 sccm. The target-to-substrate distance was kept constant at 10 cm for all

* Corresponding author.
E-mail address: ejyun@hoseo.edu (E.-J. Yun).

https://doi.org/10.1016/j.tsf.2022.139139
Received 4 December 2021; Received in revised form 26 January 2022; Accepted 13 February 2022
Available online 15 February 2022

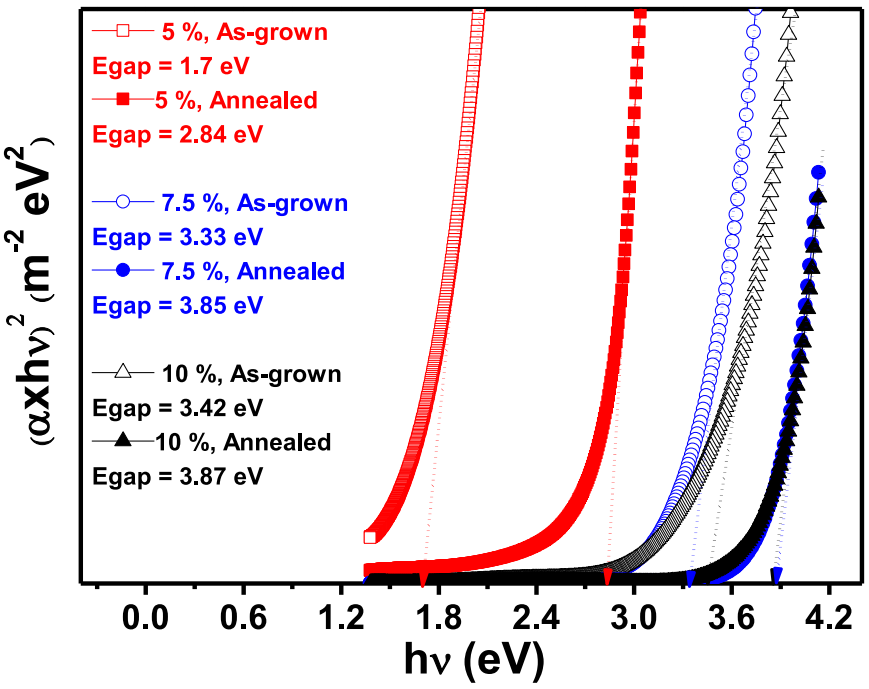

Fig. 1. (Color online) Characteristic of $(\alpha x h\nu)^2$ versus $h\nu$ of SnO_x films obtained from the results of the optical transmittance versus wavelength curves by making use of Eqs. (1) and (2). The SnO_x films were deposited at various oxygen partial pressures of 5, 7.5, and 10%. Here, the extrapolation method was used to determine optical band gap E_g.

depositions. The substrate was rotated at 2.25 rpm to deposit the SnO_x thin films with a uniform thickness. In addition, post annealing at a temperature of 300–400 °C for 30 min. was provided in an atmospheric environment inside the furnace to some as-grown SnO_x thin films for comparative purposes.

The optical band gap of the films was determined by exploring the absorption coefficient in the films at wavelengths between 300 and 900 nm, using a UV-Vis spectrophotometer (Shimadzu Co., Ltd, Japan, UV-2600i). The thicknesses of the samples were measured by using Dektak 1500 (Veeco). The electrical properties of SnO_x thin films were measured at room temperature using a Hall Effect measurement system (Ecopia, Korea, HMS-3000) according to a van der Pauw configuration.

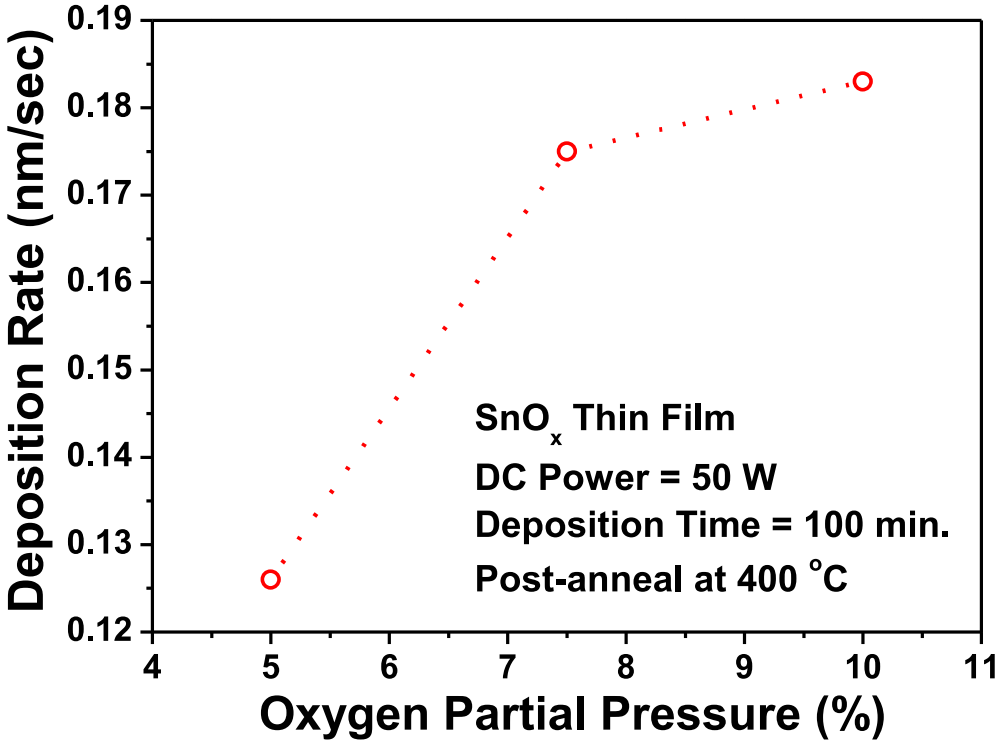

Fig. 2. Deposition rate characteristics as a function of oxygen partial pressure (OPP) for SnO_x films deposited using 50 W direct-current power and 100 min deposition time and post annealed at 400°C.

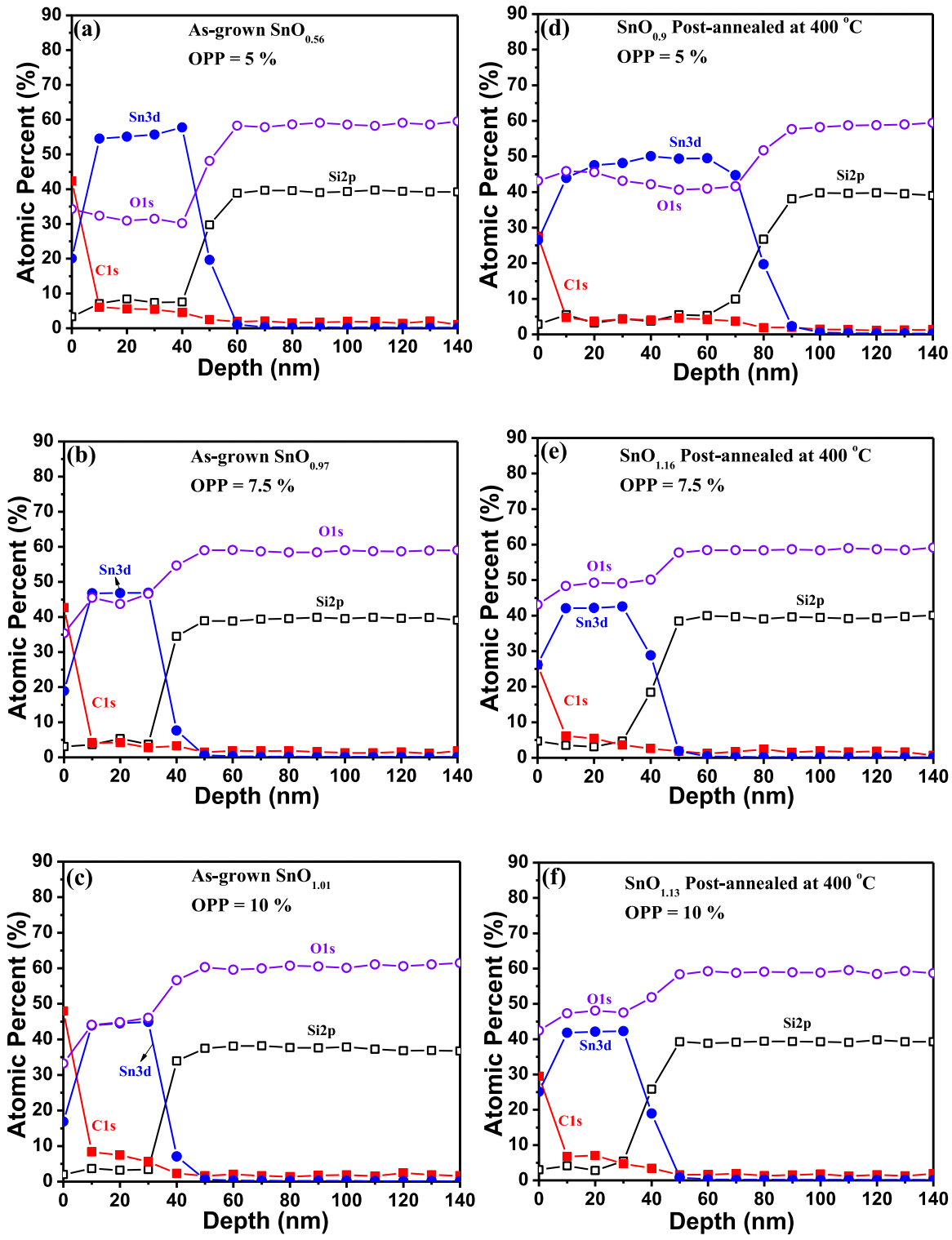

Fig. 3. (Color online) Atomic percentage changes in Sn 3d, O 1s, Si 2p, and C 1s concentrations in as-grown SnO_x thin films prepared at (a) 5, (b) 7.5, and (c) 10% oxygen partial pressure (OPP), and in SnO_x thin films fabricated at (d) 5, (e) 7.5, and (f) 10% OPP and then annealed at 400°C, which were obtained from X-ray photoelectron spectroscopy depth profiles.

The structures of the films were characterized by high resolution X-ray diffraction (HR-XRD) (Rigaku-Smartlab, Japan) of Bragg–Brentano geometry with a Cu $K\alpha_1$ radiation source ($\lambda = 0.15418$ nm). The atomic percentage changes in the depth profiles and chemical bonding states of Sn and O in the SnO_x thin films were analysed by X-ray photoelectron spectroscopy (XPS) (Thermo Fisher Scientific, USA, K-Alpha). XPS data were recorded after in-situ etching of the surface with 1 keV Ar+ ions bombardment for 20 sec. Samples were analyzed by XPS using an Al Kα x-ray ($h\nu = 1486.6$ eV) source. The surface morphologies and compositions of the films were directly observed on the films by scanning electron microscopy (SEM) (Tescan, Czech, LYRA3) at an operating voltage of 10 kV, a working distance of 9 mm, and a magnification of 100 kX without any kind of sample preparation.

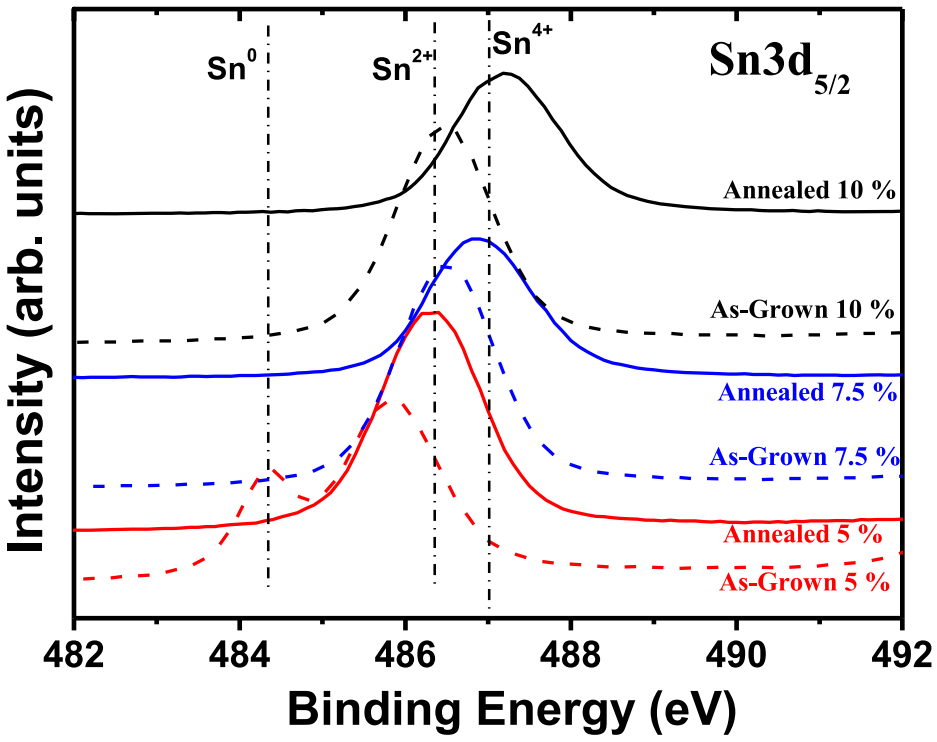

Fig. 4. (Color online) Typical Sn $3d_{5/2}$ narrow-scan X-ray photoelectron spectroscopy spectra compared using three Sn peaks in the SnO_x thin films deposited at different oxygen partial pressures, 5, 7.5, and 10%, without and with post-annealing at 400 °C.

3. Results and discussion

Since photons with energies less than the optical band gap are transmitted, the results of the optical transmittance (T) versus wavelength (λ) curves of SnO_x films gives an accurate measure of the band gap energy. The optical band gap energy was determined using the following Tauc formula for direct allowed transitions given by Refs [33–36].:

$$(\alpha \times \ h\nu)^2 = A\left(h\nu - E_g\right), \tag{1}$$

where α is the absorption coefficient of SnO_x films, h is Planck's constant, ν is the photon's frequency, A is a proportionality constant, and E_g is the optical band gap energy of SnO_x films. Here α can be estimated using the following equations [37]:

$$\alpha \approx \frac{1}{d}\ln\left(\frac{1}{T}\right), \tag{2}$$

where T is the transmittance and d is the thickness of SnO_x films.

Fig. 1 shows the $(\alpha \times h\nu)^2$ versus hν curves of SnO_x films obtained from the results of the optical T versus λ curves of SnO_x films prepared in this study by making use of Eqs. (1) and (2). In Fig. 1, the extrapolation method [38] was used to determine E_g. As shown in Fig. 1, as-grown SnO_x films deposited at OPPs of 5, 7.5 and 10% had lower band gaps of 1.7, 3.33, and 3.42 eV, while those prepared at OPPs of 5, 7.5, and 10% and post annealed at 400 °C had larger band gaps of 2.84, 3.85, and 3.87 eV, respectively. It is well known [7,39,40] that the SnO phase is p-type with band gaps of 2.7–3.4 eV, while the SnO_2 phase is n-type with band gaps of 3.6–3.8 eV. Therefore, this suggests that as–grown samples deposited at OPPs of 7.5 and 10% and post-annealed samples deposited at an OPP of 5% had a p-type SnO phase, while samples fabricated at OPPs of 7.5 and 10% and post annealed at 400 °C had a n-type SnO_2 phase. In addition, Fig. 1 shows that post annealing at 400 °C shifts the optical band gap to the right, thus increasing the band gap.

Fig. 2 shows the deposition rate characteristics as a function of OPP for SnO_x films deposited using 50 W DC power and 100 min deposition time and post annealed at 400 °C Fig. 2. indicates that the deposition rate increases with increasing the OPP. The increase in the deposition rate with a higher OPP can be explained as follows. In general, during the deposition process, sputtered Sn atoms ejected from the Sn target by energetic sputtering Ar atoms can deposit on the substrates. At higher OPPs, the collision of the sputtered Sn atoms with the oxygen atoms increases, resulting in the decrease in the deposition rate of SnO_x films. On the other hand, the electronegativity difference between Sn^{4+} (1.706) and O (3.758) is large [41]. This strong binding of Sn to O makes it easier for Sn atoms to diffuse into the SnO_x films during the sputtering process, which causes the increase in the deposition rate of SnO_x films with a higher OPP. Therefore, in our case, we conclude that the large electronegativity difference between Sn and O overwhelms the number of collisions between sputtered Sn and oxygen atoms, leading to an increase in the deposition rate of SnO_x thin films with higher OPP. According to the results of ref [42]., up to about 5 sccm O_2, OPP remains low due to the getter effect of the metal. In this elemental mode, the average sputtering yield of the target is close to that of pure metal, and deposition of metal oxides that are less dense than metal occurs, increasing the deposition rate as the OPP increases. On the other hand, at O_2 above 6 sccm, the target operates in reactive sputtering mode with a high level of OPP, which reduces the deposition rate with increasing OPP. Therefore, we believe that in our case using 2 – 4 sccm O_2, the target operates in elemental mode with low levels of OPP, increasing the deposition rate with increasing OPP, as shown in Fig. 2.

Fig. 3a, b, and c show XPS depth profiles which exhibit atomic percentage changes in Sn 3d, O 1s, Si 2p, and C 1s concentrations in as-grown SnO_x thin films prepared at OPPs of 5, 7.5, and 10%. As shown in Fig. 3, with increasing OPP from 5 to 7.5%, the atomic percentage value of the Sn content decreased from 56 to 47% while the atomic percentage value of the O content increased from 31 to 45%. During the deposition process, Sn atoms released from the target by Ar atoms sputtered with energy can be deposit on the substrate. At higher OPPs, the collision of sputtered Sn atoms with oxygen atoms increases,

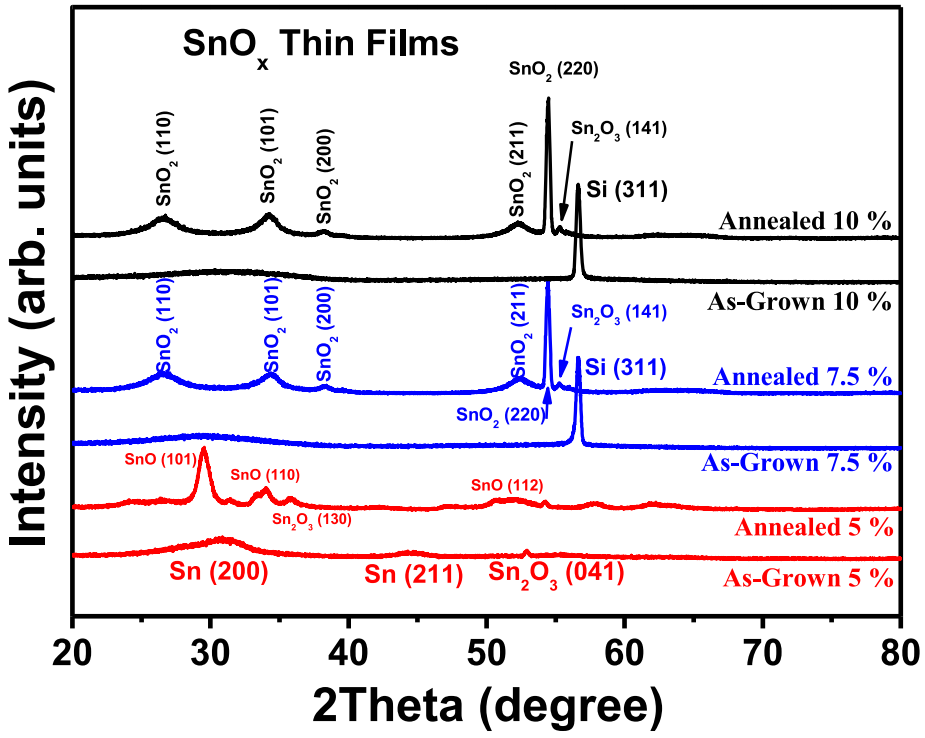

Fig. 5. (Color online) High resolution X-ray diffraction patterns of SnO_x films deposited at different oxygen partial pressures, 5, 7.5, and 10%, without and with post-annealing at 400 °C.

resulting in the formation of SnO_x films with less Sn and more O content. However, even when the OPP was further increased to 10%, the atomic percentage values of oxygen and Sn contents were almost constant[1] Fig. 3. also shows the composition ratio of tin and oxygen elements according to the XPS depth profile analysis. As-grown samples with OPPs of 5, 7.5, and 10% had composition ratios of tin and oxygen elements of 1:0.56, 1:0.97, and 1:1.01, confirming that they had composition ratios of $SnO_{0.56}$, $SnO_{0.97}$, and $SnO_{1.01}$, respectively. Therefore, from the results in Fig. 3a, b, and c, we conclude that the compositional transition from Sn-rich metallic $SnO_{0.56}$ to p-type SnO occurs as the OPP increases from 5 to 7.5%. This is in good agreement with the E_g result shown in Fig. 1.

Fig. 3d, e, and f also show atomic percentage changes in Sn 3d, O 1s, Si 2p, and C 1s concentrations in SnO_x thin films fabricated at 5, 7.5, and 10% OPP and then annealed at 400°C, which were obtained from XPS depth profiles. For samples prepared with 5% OPP, as can be seen from the results in Fig. 3a and d, after post-annealing at 400°C for 30 min, the composition of the sample changed from Sn-rich metal $SnO_{0.56}$ to p-type $SnO_{0.9}$. In contrast, the composition of the samples fabricated at 7.5 and 10% higher OPP was converted from p-type SnO to oxygen-enriched n-type $SnO_{1.2}$ after post-annealing at 400°C. Therefore, we conclude from the results in Fig. 3 that post-annealing in air at 400°C introduces more oxygen into the sample, resulting in a more oxidized sample.

All XPS binding energies were calibrated using the a carbon (C) 1s reference peak centered at 284.6 eV. The Sn $3d_{5/2}$ narrow-scan XPS spectra of SnO_x thin films were detected at binding energies of 484.3 to 487 eV [15–17,24,25,27,30] and were compared using three Sn peaks related to Sn^0, Sn^{2+}, and Sn^{4+} peaks centered at about 484.3, 486.3, and 487 eV, respectively, corresponding to metallic Sn, p-type SnO, and n-type SnO_2[2] Fig. 4. shows typical Sn $3d_{5/2}$ narrow-scan XPS spectra compared using three Sn peaks in the SnO_x thin films deposited at different OPPs, 5, 7.5, and 10%, without and with post-annealing at 400 °C. As shown in Fig. 4, for as-grown SnO_x films prepared at an OPP of 5 % without post-annealing, a metallic Sn^0 peak at ~484.3 eV and a Sn peak at 485.8 eV were observed, suggesting the presence of multiple phases of tin-rich SnO_x in the films. As OPP increased to 7.5 and 10 %, the Sn^{2+} peak at the ~486.4 eV position grew and dominated the whole, while a Sn^0 peak at ~484.3 eV and a Sn peak at 485.8 eV disappeared, indicating that a single phase of p-type SnO exists in the films. Therefore, Fig. 4 shows that the phase transition from tin-rich SnO_x to p-type SnO occurs with increasing OPP from 5 to 7.5 and 10 % for as-grown SnO_x films.

The effect of 400°C post heat treatment in air on the phase in the SnO_x thin film was studied, which is also well shown in Fig. 4. As shown in Fig. 4, in the case of the SnO_x thin films deposited with an OPP of 5 %, after 400°C heat treatment, a Sn^0 peak at ~484.3 eV and a Sn peak at 485.8 eV disappeared and Sn^{2+} peaks at 486.3 eV appeared. This suggests that the phase transition from tin-rich SnO_x to p-type SnO occurs after post heat treatment for samples deposited with an OPP of 5 %. On the other hand, in the case of the SnO_x films deposited with OPPs of 7.5 and 10 %, after post heat treatment, a Sn^{2+} peak at 486.4 eV disappeared and a Sn^{4+} peak at 487 eV appeared. This suggests that the phase transition from p-type SnO to n-type SnO_2 occurs after post heat treatment for samples deposited with OPPs of 7.5 and 10 %. It can be seen from Fig. 4 that the post annealing at 400°C resulted in a higher amount of oxygen injected into the SnO_x thin film. This is in good agreement with the E_g and XPS results in Fig. 1 and Fig. 3, respectively.

Fig. 5 shows the HR-XRD patterns of SnO_x films deposited at different OPPs, 5, 7.5, and 10%, without and with heat treatment at 400°C. As shown in Fig. 5, the as-grown samples with 5% OPP without annealing exhibited two broad halo peaks centered at 30.87 and 44.67° 2θ, which were assigned to Sn(200) and Sn(211) phases, respectively [43,44] and a small peak centered at 52.94° 2θ, which was related to a Sn_2O_3(041) phase [45,46]. This indicates that Sn-rich metallic SnO_x films were deposited for the samples prepared at 5% OPP and without

[1] Put period (.) here.
[2] Put a period here.

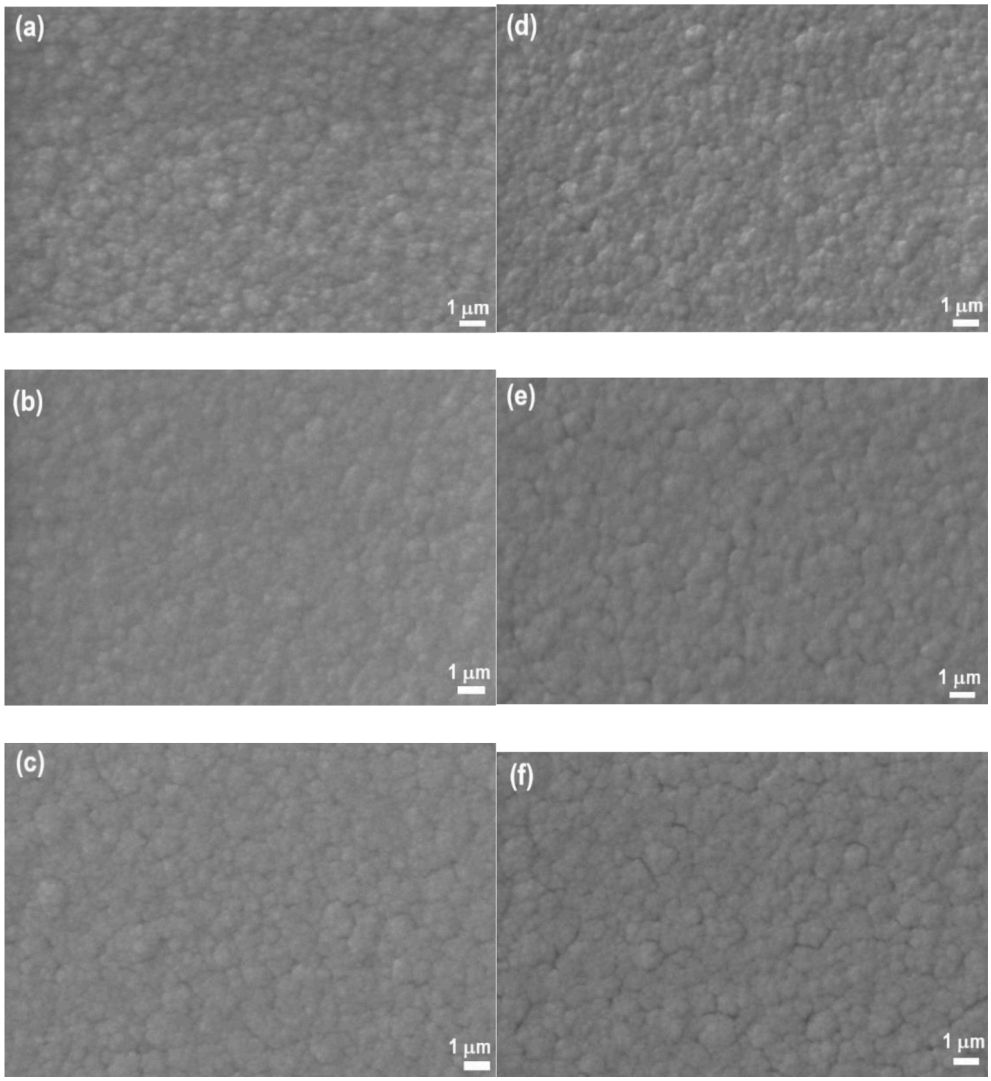

Fig. 6. Scanning electron microscopy top images of as-grown SnO_x thin films prepared at (a) 5, (b) 7.5, and (c) 10% oxygen partial pressure (OPP), and SnO_x thin films fabricated at (d) 5, (e) 7.5, and (f) 10% OPP and then annealed at 400°C.

post-annealing, which supports the XPS results shown in Fig 3a[3] Fig. 5. also shows that as the OPP increases from 5 to 7.5%, these Sn halo peaks and a Sn_2O_3 peak weaken and disappear, and only one sharp Si(311) peak centered at 56.64°2θ [47] attributed to the Si substrate appears. The same situation persisted even after raising the OPP to 10%. This suggests that only the amorphous phase is present in the samples deposited at 7.5 and 10% OPP and not post-annealed. The adatom mobility and the reactions between Sn and O are restricted on the unheated substrate surface during deposition, which induces a large number of defects in the SnO_x films. Therefore, very fine nanocrystalline or amorphous films are formed. Fig. 5. also exhibited that after the samples with 5% OPP were post-annealed at 400°C they revealed one strong peak centered at 29.54° 2θ and two small broad halo peaks centered at 33.39 and 50.94° 2θ, which were assigned to SnO(101), SnO (110), and SnO(112) phases, respectively [15–18,30,43–45,48,49] and five small halo peaks at 26.45, 34.02, 54.28, 57.97, and 62.26° 2θ, which were attributed to a SnO_2(110), SnO_2(101), SnO_2(220), SnO_2(002), and SnO_2(310) phases [15–18,30,43,45,50], respectively. This suggests that the p-type SnO phase predominates in the samples prepared in 5% OPP and post-annealed, which supports the XPS results shown in Fig. 3d. On the other hand, for the samples made with 7.5 and 10% OPP, due to post-annealing at 400°C, a strong and sharp SnO_2(220) peak appears at 54.43° 2θ, and four small SnO_2(110), SnO_2(101), SnO_2(200), and SnO_2(211) halo peaks appear at 26.88, 34.38, 38.41 and 52.32° 2θ, respectively [15–18,30,43,45,50]. This confirms that the phase formation of n-type SnO_2 occurs for samples fabricated at 7.5 and 10% OPP and post-annealed at 400°C. All the Sn, SnO, SnO_2, Sn_2O_3, Sn_3O_4, and Si diffraction peaks in Fig. 5 were indexed using JCPDS cards # 86-2265, # 06-0395, # 41-1445(or # 78-1063), # 25-1259, # 20-1293, and # 27-1402, respectively. It is worth noting that the XRD results shown in Fig. 5 are also in good agreement with the XPS results in Figs. 3 and 4 and the E_g results in Fig. 1.

Fig. 6 shows SEM top images of SnO_x films deposited at different OPPs, 5, 7.5, and 10%, without and with heat treatment at 400°C as a function of OPP. As can be seen, the films made with higher OPPs had a smoother surface morphology. This suggests that the higher the OPP, the greater the amount of oxygen injected into the SnO_x thin film, leading to the growth of crystal grains. The results also indicate that the various grain sizes (the lateral lengths of the grain sizes ranged from 1 to 2 μm) were mixed with each other; in particular, the grains overlapped each other and some large grains consisted of many smaller ones. However, all films had similarly sized grains regardless of post annealing at 400°C.

Table 1 shows Hall effect measurements representing the electrical

[3] Put a period here.

Table 1
(Color online) Summary of the Hall-Effect measurement results for the series of SnO_x samples prepared in this study

Oxygen Partial Pressure of samples (%)	Post-annealing	Resistivity (Ω·cm)	Hall mobility [$cm^2/(V·s)$]	Carrier concentration ($1/cm^3$)	Type of Semiconductor
5	No	990.4	5.47	1.15×10^{15}	n
5	Yes	1.05	0.11	5.4×10^{19}	p
7.5	No	1082	5.11	1.13×10^{15}	p
7.5	Yes	0.20	0.35	8.82×10^{19}	n
10	No	998.9	2.09	2.99×10^{15}	p
10	Yes	0.12	0.59	9.23×10^{19}	n

properties of a series of SnO_x samples prepared in this study. As listed in Table 1, as-grown samples deposited at 7.5 and 10% OPP and not post-annealed and post-annealed samples with 5% OPP exhibited p-type conductivity. However, as-grown samples deposited at 5% OPP and not post-annealed and post-annealed samples with 7.5 and 10% OPP showed n-type conductivity. The inverse transformation mechanism of the carrier type can be described as follows. Post-annealing in air at 400°C for 30 min introduces more oxygen to the sample, resulting in a more oxidized sample as confirmed by the XPS data shown in Fig. 3. Therefore, for samples prepared with 5% OPP, after post-annealing, the carrier type of the sample was changed from n-type Sn-rich $SnO_{0.56}$ to p-type SnO. In contrast, oxidation of samples by post-annealing caused carrier transitions from p-type SnO to oxygen-enriched n-type SnO_2 for samples fabricated at 7.5 and 10% OPP.

Table 1 also shows that the samples have highly conductive properties with much higher carrier concentration, low resistivity, and low mobility after post annealing at 400°C. This is caused by the growth of crystallites due to post annealing. Therefore, without post-annealing, the carrier concentration of the SnO_x thin film decreased by four orders of magnitude, which decreased carrier scattering and, as a result, significantly increased the mobility of the sample. As indicated in Table 1, the SnO_x thin films deposited at 7.5% OPP and not heat treated showed the best p-type electrical properties, with a Hall mobility of 5.11 cm^2/Vs, a hole carrier concentration of 1.13×10^{15} cm^{-3}, and a resistivity of 1082 Ωcm.

4. Conclusion

In this study, the effect of oxygen partial pressure on the properties of SnO_x thin films deposited by DC magnetron sputtering using a Sn metal target was investigated. As-grown samples deposited at 7.5 and 10% OPP and post-annealed samples deposited at 5% OPP had a p-type SnO phase, as confirmed by optical bandgap, XPS, HR-XRD and Hall effect measurements. On the other hand, samples fabricated from 7.5 and 10% OPP and annealed at 400°C had a n-type SnO_2 phase. Annealing at 400°C shifts the optical bandgap to the right, increasing the bandgap and injecting more oxygen into the SnO_x thin film, which further oxidizes the sample. In addition, post-annealing increased the carrier concentration of the SnO_x thin film by four orders of magnitude, which increased carrier scattering and, as a result, greatly reduced the mobility of the sample. The SnO_x thin film deposited at 7.5% OPP and not heat treated showed the best p-type electrical properties, with a Hall mobility of 5.11 cm^2/Vs, a hole carrier concentration of 1.13×10^{15} cm^{-3}, and a resistivity of 1082 Ωcm.

CRediT authorship contribution statement

J.S. Jung: Conceptualization, Methodology, Investigation. **S.J. Park:** Validation, Investigation, Formal analysis. **J.H. Ye:** Data curation. **J.G. Woo:** Resources. **B.S. Bae:** Resources, Supervision. **E.-J. Yun:** Visualization, Investigation, Writing – original draft, Writing – review & editing, Funding acquisition.

Declaration of Competing Interest

The authors declare that they have no known competing financial interests or personal relationships that could have appeared to influence the work reported in this paper.

Acknowledgments

This study was supported by the Basic Science Research Program through the National Research Foundation of Korea (NRF) funded by the Ministry of Education (NRF-2019R1D1A3A0310351513)

References

[1] Z. Ma, W. Zhou, Z. Xiao, H. Zhang, Z. Li, J. Zhuang, C. Peng, Y. Huang, Negligible hysteresis planar perovskite solar cells using Ga-doped SnO_2 nanocrystal as electron transport layers, Org. Electron. 71 (2019) 98–105, https://doi.org/10.1016/j.orgel.2019.05.011.
[2] T. Mohammad, V. Kumar, V. Dutta, Spray deposited indium doped tin oxide thin films for organic solar cell application, Phys. E: Low-Dimens. Syst. Nanostruct. 117 (2020), 113793, https://doi.org/10.1016/j.physe.2019.113793.
[3] U. Farva, J. Kim, Growth temperature-dependent morphological, optical, and electrical study of SnO_2 thin film by atomic layer deposition, Mater. Chem. Phys. 267 (2021), 124584, https://doi.org/10.1016/j.matchemphys.2021.124584.
[4] M. Kumar, S.S.A. Askari, M.K. Das, Some studies on surface morphological properties of SnO_x thin film layer grown by e-beam technique under controlled oxygen pressure, Mater. Today 43 (2021) 3658–3661, https://doi.org/10.1016/j.matpr.2020.09.839.
[5] T.N.L. Tran, A. Szczurek, S. Varas, C. Armellini, F. Scotognella, A. Chiasera, M. Ferrari, G.C. Righini, A. Lukowiak, Rare-earth activated SnO_2 photoluminescent thin films on flexible glass: synthesis, deposition and characterization, Opt. Mater. 124 (2022), 111978, https://doi.org/10.1016/j.optmat.2022.111978.
[6] J. Zhao, X. Ding, J. Miao, J. Hu, H. Wan, S. Zhou, Improvement in light output of ultraviolet light-emitting diodes with patterned double-layer ITO by laser direct writing, Nanomaterials 9 (2) (2019) 203, https://doi.org/10.3390/nano9020203.
[7] T. Le, H.P. Dang, A.Q. Duong, Q.H. Luc, Effect of Sn-substituted Ga and In dopant content on the structural, electrical, and optical properties of p-type X-doped SnO_2 (X = Ga and In) films: Testing the photoelectronic effect of X-doped SnO_2/n-Si junctions, J. Photochem. Photobiol. A: Chem. 376 (2019) 88–99, https://doi.org/10.1016/j.jphotochem.2019.03.003.
[8] A.A. Abuelwafa, M.S. Abd El-sadek, S. Elnobi, T. Soga, Effect of transparent conducting substrates on the structure and optical properties of tin (II) oxide (SnO) thin films: comparative study, Ceram. Int. 47 (2021) 13510–13518, https://doi.org/10.1016/j.ceramint.2021.01.209.
[9] Y. Yuan, S. Dai, S. Yan, D. Bao, Y. Wang, J. Zhang, Y. Li, Q. Wang, Q. Xin, A. Song, Imaging array and complementary photosensitive inverter based on P-Type SnO thin-film phototransistors, IEEE Electron Device Lett 42 (7) (2021) 1010–1013, https://doi.org/10.1109/LED.2021.3078616.
[10] M.A. Sayeed, H.K. Rouf, Al-doped SnO_2 thin films: impacts of high temperature annealing on the structural, optical and electrical properties, J. Mater. Res. Technol. 15 (2021) 3409–3425, https://doi.org/10.1016/j.jmrt.2021.09.145.
[11] E. Fortunato, P. Barquinha, R. Martins, Oxide semiconductor thin-film transistors: a review of recent advances, Adv. Mater. 24 (22) (2012) 2945–2986, https://doi.org/10.1002/adma.201103228.
[12] L. Qiang, W. Liu, Y. Pei, G. Wang, R. Yao, Trap states extraction of p-channel SnO thin-film transistors based on percolation and multiple trapping carrier conductions, Solid-State Electron 129 (2017) 163–167, https://doi.org/10.1016/j.sse.2016.11.010.
[13] J.-H. Lee, Y.-J. Choi, C.-Y. Jeong, D.-K. Jung, S. Ham, H.-I. Kwon, Electrical instability of p-channel SnO thin film transistors under light illumination, IEEE Electron Dev. Lett. 37 (3) (2016) 295–298, https://doi.org/10.1109/LED.2016.2516578.
[14] A. Azmi, J. Lee, T.J. Gim, R. Choi, J.K. Jeong, Performance improvement of p-channel tin monoxide transistors with a solution-processed zirconium oxide gate dielectric, IEEE Electron Dev. Lett. 38 (11) (2017) 1543–1546, https://doi.org/10.1109/LED.2017.2758349.
[15] L. Guo, M. Zhao, D. Zhuang, Q. Gong, H. Tan, M. Cao, L. Ouyang, A study on phase transformation of SnO_x thin films prepared by reactive magnetron sputtering,

Mater. Sci. Semicond. Process. 46 (2016) 35–38, https://doi.org/10.1016/j.mssp.2015.10.008.
[16] P.-C. Chen, Y.-C. Chiu, Z.-W. Zheng, C.-H. Cheng, Y.-H. Wu, Influence of plasma fluorination on p-type channel tin-oxide thin film transistors, J. Alloys Compd. 707 (2017) 162–166, https://doi.org/10.1016/j.jallcom.2016.11.294.
[17] H. Luo, L. Liang, H. Cao, Carrier trapping anisotropy in ambipolar SnO thin-film transistors, Solid State Electron 129 (2017) 88–92, https://doi.org/10.1016/j.sse.2017.01.001.
[18] J.S. Ahn, R. Pode, K.B. Lee, Study of Cu-doped SnO thin films prepared by reactive co-sputtering with facing targets of Sn and Cu, Thin Solid Films 608 (2016) 102–106, https://doi.org/10.1016/j.tsf.2016.04.024.
[19] Y. Ogo, H. Hiramatsu, K. Nomura, H. Yanagi, T. Kamiya, M. Hirano, H. Hosono, p-channel thin-film transistor using p-type oxide semiconductor, SnO, Appl. Phys. Lett. 93 (2008), 032113, https://doi.org/10.1063/1.2964197.
[20] L.Y. Liang, Z.M. Liu, H.T. Cao, Z. Yu, Y.Y. Shi, A.H. Chen, H.Z. Zhang, Y.Q. Fang, X. L. Sun, Phase and optical characterizations of annealed SnO thin films and their p-type TFT application, J. Electrochem. Soc. 157 (6) (2010) H598–H602, https://doi.org/10.1149/1.3385390.
[21] J. Um, B.M. Roh, S. Kim, S.E. Kim, Effect of radio frequency power on the properties of p-type SnO deposited via sputtering, Mater. Sci. Semicond. Process. 16 (6) (2013) 1679–1683, https://doi.org/10.1016/j.mssp.2013.03.009.
[22] P.-C. Hsu, W.-C. Chen, Y.-T. Tsai, Y.-C. Kung, C.-H. Chang, C.-J. Hsu, C.-C. Wu, H.-H. Hsieh, Fabrication of p-type SnO thin-film transistors by sputtering with practical metal electrodes, Jpn. J. Appl. Phys. 52 (2013) 05DC07, https://doi.org/10.7567/JJAP.52.05DC07.
[23] P.-C. Hsu, W.-C. Chen, Y.-T. Tsai, Y.-C. Kung, C.-H. Chang, C.-C. Wu, H.-H. Hsieh, Sputtering deposition of P-type SnO films using robust Sn/SnO_2 mixed target, Thin Solid Films 555 (2014) 57–61, https://doi.org/10.1016/j.tsf.2013.06.059.
[24] S.-S. Lin, Y.-S. Tsai, K.-R. Bai, Structural and physical properties of tin oxide thin films for optoelectronic applications, Appl. Surf. Sci. 380 (2016) 203–209, https://doi.org/10.1016/j.apsusc.2016.01.188.
[25] S.-S. Lin, S.-Y. Fan, Y.-S. Tsai, Effects of annealing on wettability and physical properties of SnO thin films deposited at low RF power densities, Ceram. Int. 43 (2) (2017) 1802–1808, https://doi.org/10.1016/j.ceramint.2016.10.138.
[26] H.-J. Kim, C.-Y. Jeong, S.-D. Bae, J.-H. Lee, H.-I. Kwon, Charge transport mechanism in p-channel tin monoxide thin-film transistors, IEEE Electron Dev. Lett. 38 (4) (2017) 473–476, https://doi.org/10.1109/LED.2017.2672730.
[27] J. Yang, S. Pi, Y. Han, R. Fu, T. Meng, Q. Zhang, Characteristic of bismuth-doped tin oxide thin-film transistors, IEEE Trans. Electron Devices 63 (5) (2016) 1904–1909, https://doi.org/10.1109/TED.2016.2542860.
[28] B.L. Zhu, X. Zhao, W.C. Hu, T.T. Li, J. Wu, Z.H. Gan, J. Liu, D.W. Zeng, C.S. Xie, Structural, electrical, and optical properties of F-doped SnO or SnO_2 films prepared by RF reactive magnetron sputtering at different substrate temperatures and O_2 fluxes, J. Alloys Compd. 719 (2017) 429–437, https://doi.org/10.1016/j.jallcom.2017.05.193.
[29] A.Q. Duong, H.P. Dang, T. Le, Studying and fabricating optical, electrical, and structural properties of p-type Al- and N- co-doped SnO_2 (ANTO) films and investigating the photo-electro effect of p-ANTO/n-Si heterojunctions, J. Photochem. Photobiol. A 390 (2020), 112334, https://doi.org/10.1016/j.jphotochem.2019.112334.
[30] A.H.-T. Nguyen, M.-C. Nguyen, J. Choi, S. Han, J. Kim, R. Choi, Electrical performance enhancement of p-type tin oxide channel thin film transistor using aluminum doping, Thin Solid Films 641 (2017) 24–27, https://doi.org/10.1016/j.tsf.2017.01.032.
[31] T.J. Yen, A. Chin, V. Gritsenko, Exceedingly high performance top-gate p-type SnO thin film transistor with a nanometer scale channel layer, Nanomaterials 11 (1) (2021) 92, https://doi.org/10.3390/nano11010092.
[32] H.-M. Kim, S.-H. Choi, H.J. Jeong, J.-H. Lee, J. Kim, J.-S. Park, Highly dense and stable p-type thin-film transistor based on atomic layer deposition SnO fabricated by two-step crystallization, ACS Appl. Mater. Interfaces 13 (26) (2021) 30818–30825, https://doi.org/10.1021/acsami.1c06038.
[33] A.H. Shukor, H.A. Alhattab, I. Takano, Electrical and optical properties of copper oxide thin films prepared by DC magnetron sputtering, J. Vac. Sci. Technol. B 38 (1) (2020), 012803, https://doi.org/10.1116/1.5131518.
[34] B.D. Viezbicke, S. Patel, B.E. Davis, D.P. Birnie, Evaluation of the Tauc method for optical absorption edge determination: ZnO thin films as a model system, Phys. Status Solidi B 252 (8) (2015) 1700–1710, https://doi.org/10.1002/pssb.201552007.
[35] J. Tauc, R. Grigorovici, A. Vancu, Optical properties and electronic structure of amorphous germanium, Phys. Status Solidi 15 (2) (1966) 627–637, https://doi.org/10.1002/pssb.19660150224.
[36] E.A. Davis, N.F. Mott, Conduction in non-crystalline systems V. Conductivity, optical absorption and photoconductivity in amorphous semiconductors, Philos. Mag. 22 (179) (1970) 903–922, https://doi.org/10.1080/14786437008221061.
[37] A. Moumen, B. Hartiti, E. Comini, Z. El khalidi, H.M.M.M. Arachchige, S. Fadili, P. Thevenin, Preparation and characterization of nanostructured CuO thin films using spray pyrolysis technique, Superlattices Microstruct. 127 (2019) 2–10, https://doi.org/10.1016/j.spmi.2018.06.061.
[38] E.-J. Yun, J.W. Jung, Y.H. Han, M.-W. Kim, B.C. Lee, Effect of high-energy electron beam irradiation on the transmittance of ZnO thin films on transparent substrates, J. Korean Phys. Soc. 56 (2010) 356–361, https://doi.org/10.3938/jkps.56.356.
[39] J.-S. Park, D.-Y. Kim, W.-B. Kim, I.-K. Park, Realization of Eu-doped p-SnO_2 thin film by spray pyrolysis deposition, Ceram. Int. 46 (1) (2020) 430–434, https://doi.org/10.1016/j.ceramint.2019.08.279.
[40] J. Jia, T. Sugane, S.-I. Nakamura, Y. Shigesato, p-type conduction mechanism in continuously varied non-stoichimetric SnO_x thin films deposited by reactive sputtering with the impedance control, J. Appl. Phys. 127 (2020), 185703, https://doi.org/10.1063/5.0005953.
[41] K. Li, D. Xue, Estimation of electronegativity values of elements in different valence states, J. Phys. Chem. A 110 (2006) 11332–11337, https://doi.org/10.1021/jp062886k.
[42] J.F. Pierson, D. Wiederkehr, A. Billard, Reactive magnetron sputtering of copper, silver, and gold, Thin Solid Films 478 (2005) 196–205, https://doi.org/10.1016/j.tsf.2004.10.043.
[43] D.M. Jang, H. Jung, N.D. Hoa, D. Kim, S.-K. Hong, H. Kim, Tin oxide-carbon nanotube composite for NO_X sensing, J. Nanosci. Nanotechnol. 12 (2) (2012) 1425–1428, https://doi.org/10.1166/jnn.2012.4656.
[44] Z. Li, X. Tao, Y. Cheng, Z. Wu, Z. Zhang, H. Dang, A facile way for preparing tin nanoparticles from bulk tin via ultrasound dispersion, Ultrason. Sonochem. 14 (1) (2007) 89–92, https://doi.org/10.1016/j.ultsonch.2005.11.008.
[45] C. Guillén, J. Herrero, P-type SnO thin films prepared by reactive sputtering at high deposition rates, J. Mater. Sci. Technol. 35 (8) (2019) 1706–1711, https://doi.org/10.1016/j.jmst.2019.03.034.
[46] X. Kuang, T. Liu, W. Zeng, X. Peng, Z. Wang, Hydrothermal synthesis and characterization of novel Sn_2O_3 hierarchical nanostructures, Mater. Lett. 165 (2016) 235–238, https://doi.org/10.1016/j.matlet.2015.10.142.
[47] H.I. Bang, H.B. Seo, B.S. Bae, E.-J. Yun, Effects of oxygen ratio on the properties of tin oxide thin films doped with bismuth, Phys. Status Solidi A 216 (2019), 1800863, https://doi.org/10.1002/pssa.201800863.
[48] L.Y. Liang, Z.M. Liu, H.T. Cao, X.Q. Pan, Microstructural, optical, and electrical properties of SnO thin films prepared on quartz via a two-step method, ACS Appl. Mater. Inferfaces 2 (2010) 1060–1065, https://doi.org/10.1021/am900838z.
[49] X. Chu, X. Zhu, Y. Dong, W. Zhang, L. Bai, Formaldehyde sensing properties of SnO–graphene composites prepared via hydrothermal method, J. Mater. Sci. Technol. 31 (9) (2015) 913–917, https://doi.org/10.1016/j.jmst.2015.05.001.
[50] D.M. Mukhamedshina, N.B. Beisenkhanov, K.A. Mit, I.V. Valitova, V.A. Botvin, Investigation of properties of thin oxide films SnO_x annealed in various atmospheres, Thin Solid Films 495 (1-2) (2006) 316–320, https://doi.org/10.1016/j.tsf.2005.08.293.